ADVANCED FUNCTIONAL MATERIALS
www.afm-journal.de

Direct-Ink-Written Cholesteric Liquid Crystal Elastomer with Programmable Mechanochromic Response

*Jihye Choi, Yeongyu Choi, Jin-Hyeong Lee, Min Chan Kim, Sungmin Park, Kyu Hyun, Kyung Min Lee, Tae-Hoon Yoon, and Suk-kyun Ahn**

Cholesteric liquid crystal elastomers (CLCEs) are unique anisotropic rubbers that can change their structural color in response to various stimuli such as heat, chemicals, electric fields, and mechanical stress. Methods such as anisotropic deswelling and surface alignment have been adopted to prepare CLCEs; however, they have limitations in creating spatially controlled CLCE geometries. In this work, a direct ink writing (DIW)-based 3D-printable CLCE that can be prepared by extruding viscous CLC ink is developed through a 3D printer nozzle, followed by photopolymerization. Interestingly, the helical axis is inclined to the printing direction by ≈32° due to a combination of the shear-induced alignment causes during extrusion and the elongational force generated during deposition onto the substrate. This unusual helical axis distortion leads to both blue and red shifts of the reflection color depending on the direction of observation relative to the printing axis. Notably, the printed CLCE exhibits anisotropic mechanochromism upon stretching, because of the stretching-direction-dependent variations in the slant angle of the helical axis. This anisotropic mechanochromism can be harnessed to develop a unique CLCE-based strain sensor displaying intricate color patterns upon stretching, with significant application potential in encryption, anticounterfeiting, and structural health monitoring.

1. Introduction

Mechanochromic materials, which alter their nanoscale structural color in response to mechanical-stress-inducing events, such as stretching, compression, and bending, are drawing considerable attention owing to their applicability in contexts such as strain sensing,[1,2] structural health monitoring,[3,4] anticounterfeiting,[5] and encryption.[6,7] Mechanochromic materials based on the structural color can be designed to exhibit a range of optical responses, from reversible changes in color or fluorescence to more complex changes in refractive index or light scattering. This mechanochromism is a direct consequence of the deformation-induced changes in the periodic lattice constants of structurally colored materials. These structurally colored mechanochromic materials can be classified into three main groups based on their nanoscale architectures: photonic crystals,[8] photonic glass,[9] and liquid crystals (LCs).[10] Among them, LCs—which include cholesteric LCs, achiral nematic LCs, and blue-phase LCs—show considerable promise as structurally colored mechanochromic materials owing to their unique superstructures and anisotropic characteristics.[11,12]

Cholesteric liquid crystal elastomers (CLCEs) are highly deformable chiral LCEs in which the nematic director undergoes continuous rotation along the helical axis owing to chirality within the network. The distance over which the nematic director at each plane rotates completely (360°) is defined as the pitch (P). CLCEs can exhibit selective reflection at a specific wavelength (λ) that varies with the pitch, angle of incident light (θ), and average refractive index ($\langle\bar{n}\rangle$), in accordance with Bragg's law.

$$\lambda = \bar{n} \times P \cos\theta \tag{1}$$

$$\bar{n} = \frac{n_e + 2n_o}{3} \tag{2}$$

where $\bar{n}$ is the average of the ordinary and extraordinary refractive indices of the LC molecules (n_o and n_e, respectively). For a conventional planar CLCE, the longest reflected wavelength is observed when the incident light is normal to the surface of the

J. Choi, J.-H. Lee, M. C. Kim, K. Hyun, S.-kyun Ahn
School of Chemical Engineering
Pusan National University
Busan 46241, Republic of Korea
E-mail: skahn@pusan.ac.kr

Y. Choi, T.-H. Yoon
Department of Electronics Engineering
Pusan National University
Busan 46241, Republic of Korea

S. Park
Advanced Materials Division
Korea Research Institute of Chemical Technology
Daejeon 34114, Republic of Korea

K. M. Lee
Materials and Manufacturing Directorate, Air Force Research Laboratory
Wright-Patterson Air Force Base
Dayton, OH 45433, USA

K. M. Lee
Azimuth Corporation
Beavercreek, OH 45431, USA

The ORCID identification number(s) for the author(s) of this article can be found under https://doi.org/10.1002/adfm.202310658

DOI: 10.1002/adfm.202310658

cholesteric phase (that is, when $\theta = 0°$). The pitch of a CLCE is inversely proportional to the concentration ([c]) and helical twisting power (HTP; μm^{-1}) of the chiral dopant, with the HTP reflecting the strength of the chiral dopant to twist the nematic phase.

$$P = \frac{1}{[c] \times HTP} \tag{3}$$

The pitch of CLCEs can be externally manipulated, similar to their internal molecular constituents, under various stimuli such as temperature,[13] electric fields,[14] light,[11] chemicals,[15–17] and mechanical stress,[10,18,19] resulting in tunable light reflection of a broad wavelength range from ultraviolet to infrared.[2] The tunable and selective light reflection of CLCEs permits their use in developing sensors,[1–3,6] lasers,[18,20] displays,[21] and camouflage technology.[19,22]

To harness the unique chiroptical properties of CLCEs, achieving uniform orientation of the CLCE helix is critical. Kim and Finkelmann were the first to obtain a CLCE helix with uniform orientation using the "anisotropic deswelling" method, which involved intensive centrifugation during the synthesis.[23] Recently, Lagerwall and coworkers advanced the anisotropic deswelling method to make it simple, reproducible, and scalable to a millimeter-scale thickness by exploiting the strong adherence of CLCE gels to the substrate during the initial stage of the synthesis.[24] CLCEs with a uniform helix can also be obtained by polymerizing the interior of surface-aligned cells under an electric or magnetic field,[13] or by applying mechanical strain to reconfigurable CLCEs comprising dynamic covalent bonds.[19,25] Recently, Debije and coworkers reported printable CLCEs based on direct ink writing (DIW), which permitted the creation of CLCEs with complex configurations such as a butterfly-shape.[15,26,27] In this approach, the helix of the printed CLCE is inclined at a specific angle, which differentiates it from the vertical helix typically observed in conventional CLCEs. Consequently, printed CLCEs display anisotropic iridescence and polarization patterns. Similar to their optical anisotropy, the mechanochromic behavior of these printed CLCEs with slanted helices is expected to be unique and distinguishable from that of conventional CLCEs with planar alignment.

In this study, we create various custom-designed CLCEs using a two-step process involving DIW-based 3D printing and photopolymerization of CLC ink; most importantly, their anisotropic mechanochromic properties under uniaxial and biaxial stretching were investigated for the first time. Similar to previously reported systems, the printed CLCEs exhibited angle-dependent structural coloration owing to the slanted helical axis generated by the shear-induced alignment of viscous CLC ink during extrusion. Notably, anisotropic mechanochromism was observed upon stretching with respect to the printing direction, presumably owing to the stretching-direction-dependent change in the slant angle of the helical axis. The microstructural evolution of the printed CLCEs during uniaxial and biaxial stretching was revealed through UV–vis spectroscopy, X-ray scattering analysis, and polarized optical microscopy (POM). The unique anisotropic mechanochromism of the printed CLCEs was leveraged to develop an intriguing strain sensor that exhibited locally controlled color patterns upon stretching.

2. Results and Discussion

2.1. Synthesis and Characterization of CLC Ink and CLCE

The entire CLCE synthesis was conducted in melt without using any organic solvent. The CLC mixture comprised a diacrylate-functionalized LC monomer (RM257), chain extender (*n*-hexylamine), chiral dopant (S1011), and photoinitiator (I-651). The CLCE was synthesized in two steps: aza-Michael-addition-based step-growth polymerization between RM257 and *n*-hexylamine, followed by photopolymerization (**Figure 1**a). The number average molecular weight of the CLC oligomer (or CLC ink for DIW) was determined by ^{1}H NMR spectroscopy to be 4180 g mol^{-1} (Figure S1, Supporting Information). The disappearance of the acrylate peak at 810 cm^{-1} in the FTIR spectra (Figure S2, Supporting Information) and the sufficiently high gel fraction (80.1%) indicate successful preparation of CLCE. Note that extraction of the low-molecular-weight chiral dopant (S1011, 5 wt%) could lead to a decrease in the gel fraction.

The texture and phase-transition temperatures of the CLC oligomer were determined by temperature-controlled POM. To better identify the texture, the CLC oligomer was filled into a 36-µm-thick glass cell and then examined. As shown in Figure 1b, an oily streak texture of cholesteric phase and a cholesteric–isotropic transition temperature ($T_{Ch–I}$) of 55 °C are observed during cooling from the isotropic phase. The thermal transition temperatures of the CLC oligomer and CLCE were further investigated by differential scanning calorimetry (DSC; Figure 1c). The glass transition temperature (T_g) and $T_{Ch–I}$ value of the CLC oligomer were determined to be −10 and 51 °C, respectively. However, the T_g of the CLCE was estimated to be 5 °C, a value 15 °C higher than that of the CLC oligomer owing to the constricted network structure.[28,29] Investigation of the temperature-dependent modulus of the CLCE by dynamic mechanical analysis (DMA) revealed the T_g to be 29 °C, a value ≈24 °C higher than that determined by DSC (see the tan δ peak in Figure 1d). Noteworthy that our CLCE is elastomeric as it can be substantially elongated at ambient temperature as will be discussed later. The presence of a rubbery plateau suggested the existence of an efficiently formed network inside the CLCE.[30] The reflection bands of representative planar-aligned CLCE films prepared using a surface-aligned cell were clearly detected in the UV–vis spectra (Figure 1e). As expected from Equation (1) and (3), increasing the S1011 concentration in the CLCE film from 5.0 to 6.2 wt% caused a blue shift from 780 to 650 nm. It is worth noting that the same S1011 concentrations were used to prepare the DIW-printed CLCEs; the difference in optical properties of CLCEs prepared using different methods will be discussed later.

2.2. Direct-Ink-Written CLCE

The diacrylate-functionalized CLC oligomer prepared via aza-Michael addition is a highly viscous material that can be employed as an ink for DIW-based 3D printing.[31–33] To determine the rheological properties of CLC ink, temperature-dependent shear viscosity was investigated by conducting steady shear experiments. The CLC ink exhibited shear thinning behavior, suggesting that it could be aligned at high shear rates (**Figure 2**a). The shear thinning of LC melts is caused by a flow-induced

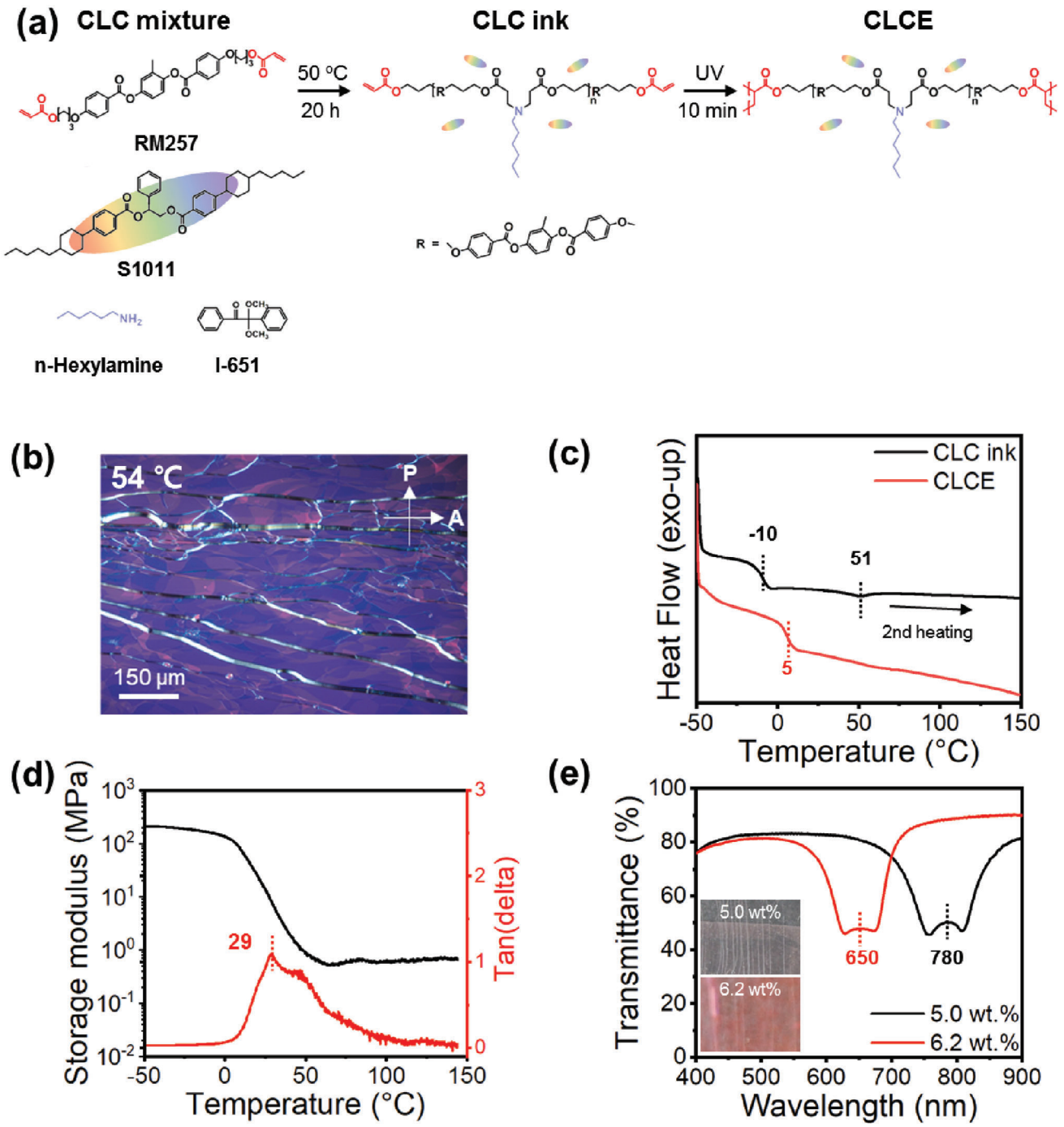

Figure 1. a) Reaction scheme of CLC ink and CLCE. b) POM image of CLC ink at 54 °C, showing its texture with oily streaks. c) DSC thermograms of CLC ink and CLCE obtained during second heating cycles at a rate of 10°C min^{-1}. d) Viscoelastic property of planar-aligned CLCE using DMA. e) Transmittance spectra and photographs of planar-aligned CLCE film doped with 5.0 and 6.2 wt% S1011.

disorder–order transition (that is, from polydomain or isotropic states to the anisotropic state).[34–36] With increasing temperature, the viscosity of CLC ink gradually decreased and the shear thinning effect weakened and eventually disappeared at 85 °C. Notably, the shear thinning persisted at temperatures above T_{Ch-I} (51 or 55 °C, as determined by DSC and POM, respectively), presumably owing to the transition between the isotropic and aligned nematic states.[36] However, CLC ink required higher shear rates to induce alignment at higher temperatures. To achieve rapid extrusion and efficient self-organization for creating a helical structure in a low-viscosity state, 75 °C (isotropic phase) and 40 °C (cholesteric phase) were selected as the printing and bed temperatures, respectively (Figure 2b). Subsequently, the printed substrate was annealed at 40 °C for 10 min to efficiently form a

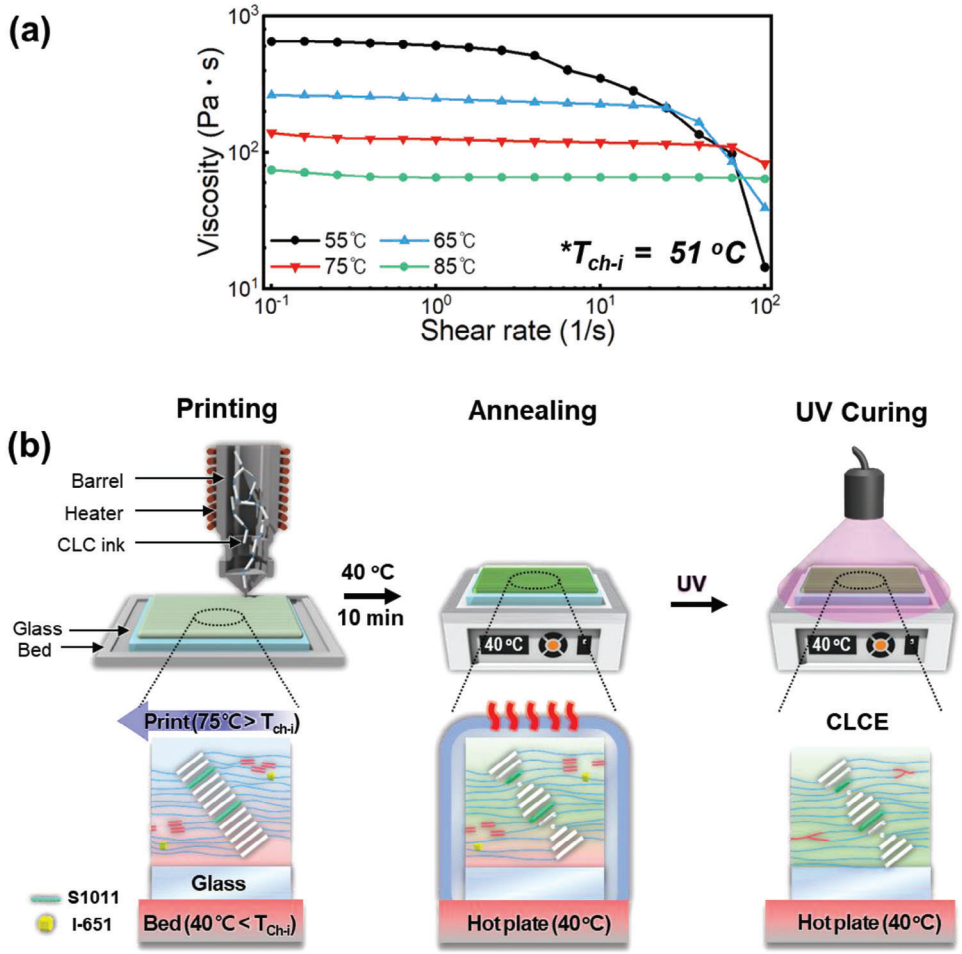

Figure 2. a) Steady shear viscosity of CLC ink as functions of shear rate and temperature. b) Schematics of the CLCE fabrication scheme, which includes printing, thermal annealing, and UV curing (top row), and the self-organized structures of CLC ink and CLCE at each fabrication step (bottom row).

stable helical structure and then photocrosslinked at 40 °C to permanently fix it through network formation. Because extrusion was performed in the isotropic phase, the cholesteric phase was achieved after several minutes of annealing at 40 °C. The annealing process can facilitate the self-assembly of mesogens into a chiral nematic phase with a more uniform CLC helix and at a faster rate, resulting in less scattering and higher transmittance (Figure S3, Supporting Information). We note that the reflected wavelength of CLCE became slightly blue-shifted after photocrosslinking due to volumetric shrinkage (Figure S4, Supporting Information). Interestingly, the helical axis of the printed CLCE was slanted at a certain angle; this will be comprehensively discussed in the subsequent section. Because the optical properties of a CLCE are highly dependent on its alignment, the sample thickness and printing conditions—such as temperature, printing speed, and pressure—had to be carefully optimized to produce a CLCE with uniform structural coloration. The optimal printing conditions were ascertained by acquiring POM images (Figure S5, Supporting Information), and the appropriate thickness range for obtaining uniform structural coloration with reasonable transmittance was estimated to be 15–60 µm (Figure S6, Supporting Information).

2.3. Anisotropic Chiroptical Properties

CLCEs exhibit unique chiroptical properties owing to their self-organized helical superstructures; therefore, controlling the helical axis is crucial for manipulating their optical properties.[37] Conventional CLCEs prepared by anisotropic deswelling or surface alignment typically aim to achieve planar alignment (that is, vertically aligning the helix with respect to the surface) to exploit the selective light reflection.[13,23,38] Alternatively, homeotropic alignment of CLCE, so-called uniformly lying helix structure, is preferred for realizing electro-optical devices[39] and switchable surface topographies.[40]

As mentioned earlier (the Figure 1e discussion), planar-aligned CLCEs were obtained using a polyimide-coated surface-aligned cell. The position of the reflection band of the CLCE doped with 6.2 wt% S1011 (650 nm) was blue-shifted at oblique viewing angles and was independent of the direction of observation (Figure S7, Supporting Information). Interestingly, the printed CLCE doped with the same amount of S1011 reflected light with a wavelength of 550 nm at normal incidence; this value is ≈100 nm lower than that of the planar-aligned CLCE (**Figure 3**a,c and Movie S1, Supporting Information). The

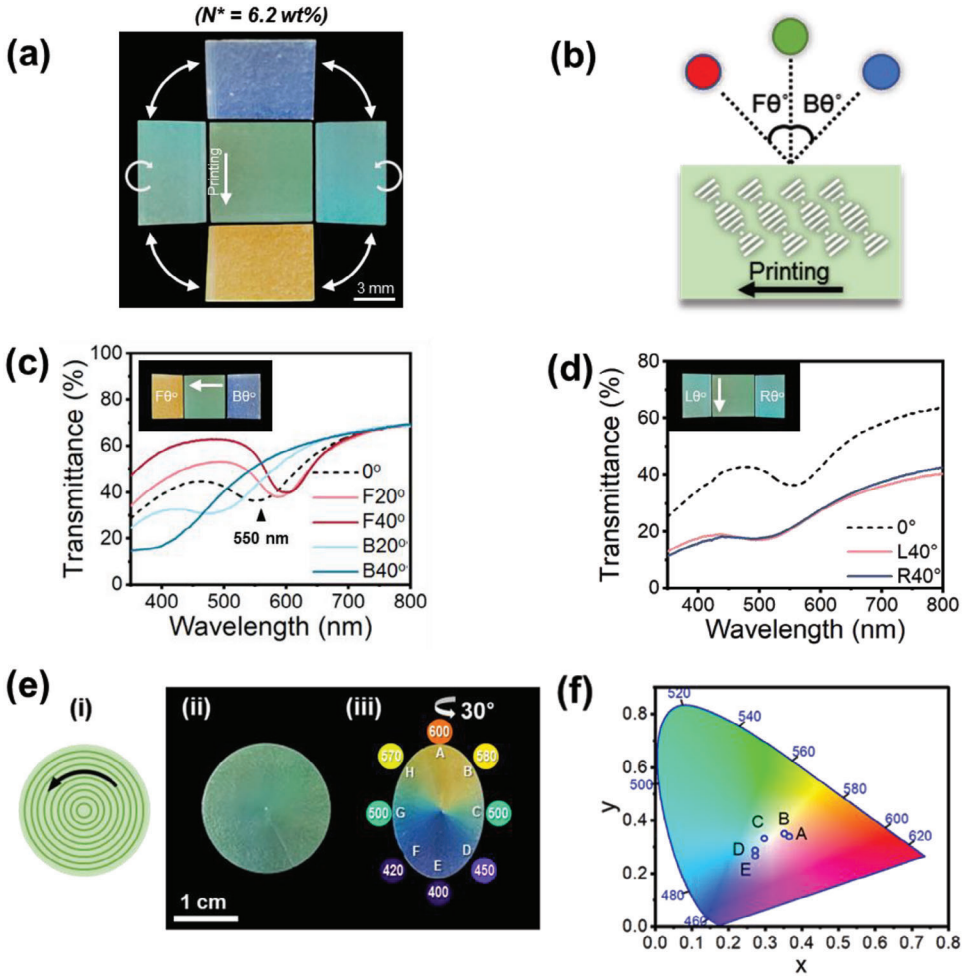

Figure 3. Optical characterization of the printed CLCE doped with 6.2 wt% S1011 (the greenish film). a) Photographs of the printed CLCE (uniaxial lines) in which the arrow in the center indicates the printing direction. Images captured in normal (center) and oblique incidence modes were acquired to visualize the angle-dependent reflection colors. b) Illustration of the printed CLCE with a slanted helical axis. The initial green reflection observed in normal incidence mode is either red- or blue-shifted when observed at oblique angles relative to the printing direction (forward (Fθ°) and backward (Bθ°)). c,d) Transmittance spectra of the printed CLCE acquired at various angles: (c) along and (d) perpendicular to the printing direction. e-i) The printing path of concentric circles. e-ii,iii) Photographs of the printed CLCE with concentric circles acquired under observation in (e-ii) normal and (e-iii) oblique incidence modes. The numbers assigned to positions "A"–"H" on the CLCE film indicate the corresponding reflected wavelength at each location. f) CIE 1931 color space diagram of the printed CLCE with concentric circles, showing the positions "A"–"E" marked in (e-iii).

spectroscopic measurements were conducted using the setup depicted in Figure S8 (Supporting Information). More interestingly, the reflected light was either red- or blue-shifted at inclined viewing angles along the printing direction. Specifically, a red or blue shift in the reflection band was observed when the sample was viewed from a forward or backward position relative to the printing direction, respectively. This unusual anisotropic light reflection (i.e., viewing-direction dependency) strongly suggested the presence of slanted helices along the printing direction instead of the conventional vertical alignment (Figure 3b). In contrast, comparable extents of blue shifts were observed at tilted viewing angles perpendicular to the printing direction (Figure 3a,d; Figure S9, Supporting Information). The slanted helical axis of the CLCE arose from the viscous nature of CLC ink and was induced by an interplay between the shear force generated during extrusion and elongational force produced during deposition on the substrate. Indeed, when the viscosity of CLC inks is reduced by diluting them with a solvent, the conventional planar alignment is obtained.[41,42] Our observation of the slanted helical axis in the CLCE is in good agreement with a recent report by Debije and coworkers, who performed a thiol–acrylate Michael reaction with a chiral mesogen (LC756) to prepare CLC ink.[26] The slant angle of our printed CLCE was calculated to be 32° (see Supporting Information for details).

The unique characteristic of the slanted helical axis in the printed CLCE enabled the creation of an interesting optical film through DIW. For instance, a concentric-circle-patterned CLCE film doped with 6.2 wt% S1011—which reflected the entire visible-light spectrum—was printed (Figure 3e). The film appeared greenish when viewed from the normal direction, whereas it reflected the full range of visible light at an oblique viewing angle (30°), owing to the combined effect of the

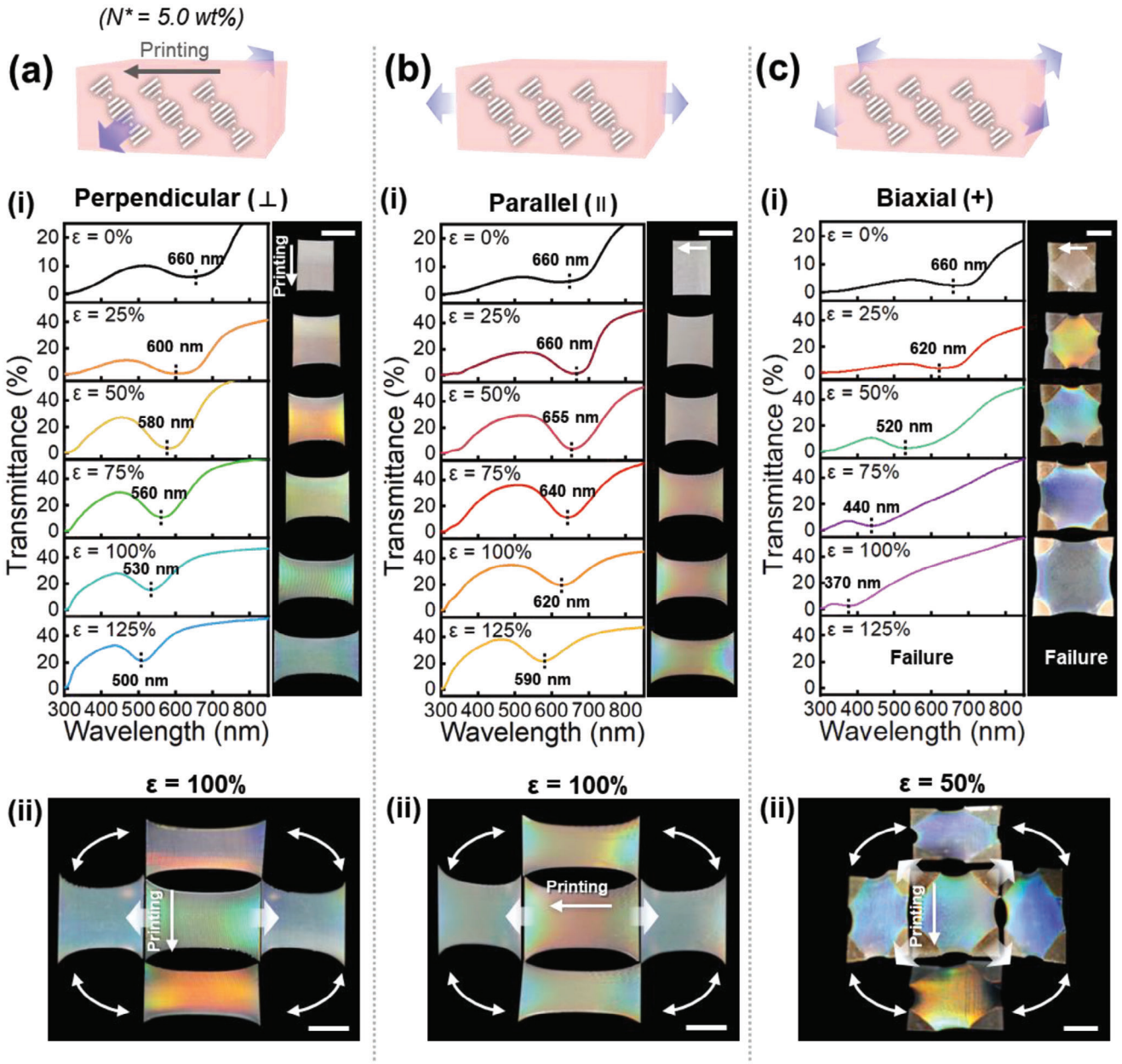

Figure 4. Mechanochromic response of the uniaxially printed CLCE doped with 5.0 wt% S1011 (a reddish film). a–c) Transmittance spectra and photographs of the printed CLCE acquired under different stretching conditions: uniaxial stretching conducted a-i) perpendicular and b-i) parallel to the printing direction, and c-i) biaxial stretching. Photographs of printed CLCE captured in normal (center) and oblique incidence modes under different stretching conditions: uniaxial stretching performed a-ii) perpendicular and b-ii) parallel to the printing direction, and c-ii) biaxial stretching.

circular printing path and anisotropic light reflection. The results of CIE 1931 color space analysis (Figure 3f) corroborated the ability of the CLCE film to reflect the entire visible-light spectrum, with each reflection point in the film labeled as "A"–"H."

2.4. Anisotropic Mechanochromic Properties

Although the mechanochromic properties of planar-aligned CLCEs have been extensively studied, CLCEs with a slanted helical axis have not yet been reported, to the best of our knowledge. The mechanochromic properties of the printed CLCE were investigated using the film doped with 5.0 wt% S1011, which exhibited red reflection (660 nm). In particular, the mechanochromic properties of the sample were examined under different deformation conditions, including uniaxial stretching along directions parallel or perpendicular to the printing trajectory, and biaxial stretching.

When uniaxial stretching was performed perpendicular to the printing direction, a considerable blue shift of the reflected light was observed from 660 to 500 nm at normal incidence as the strain increased to 125% (**Figure 4**a-i). Additionally, the reflected wavelengths of the stretched sample (ϵ = 100%) were examined

at oblique angles, which showed the same viewing-angle dependence as that exhibited by the unstretched sample, as discussed in the previous section (that is, a red or blue shift when viewed from the forward or backward direction relative to the printing trajectory; Figure 4a-ii; Figure S10, Supporting Information). The significant blue shift (150 nm) suggested a gradual decrease in the helical pitch during stretching because of the reduction in the sample thickness. However, the helices remained slanted because the reflected light continued to be dependent on the viewing direction even at strains of up to 125%.

Surprisingly, the sample uniaxially stretched parallel to the printing direction exhibited a less significant blue shift of the reflected light at normal incidence under the same 125% strain (from 660 to 590 nm; Figure 4b-i). Notably, even after 125% elongation, the middle part of the sample that experienced the least deformation retained the reddish color. This is in stark contrast to the bluish color observed in the perpendicularly stretched sample under the same strain. Furthermore, the viewing-angle dependence of the reflected wavelength along the printing direction tended to diminish with increasing strain from 0 to 100%, eventually disappearing at 125% strain (Figure 4b-ii; Figure S11, Supporting Information). The loss of the viewing-angle dependence at high strains implied that the slanted helices of the printed CLCE reoriented to the vertical direction during stretching, thereby becoming similar to a conventional planar-aligned CLCE. Consequently, when stretching was conducted parallel to the printing direction, the blue shift due to stretching (that is, a decrease in thickness) competed against the red shift caused by the decrease in slant angle. This led to a relatively smaller blue shift than that observed when stretching was performed perpendicular to the printing direction ($\Delta\lambda = 70$ and 160 nm, respectively). Notably, despite the substantial differences in the optical properties of the differently stretched CLCEs, comparable mechanical properties were observed (Figure S12, Supporting Information). This suggested that the variation in optical properties was mainly due to the structural changes and reorientation of the helical axis, rather than the overall mechanical response of the CLCE.

In addition to uniaxial stretching, the printed CLCE was subjected to biaxial stretching, which led to a significantly larger blue shift in the reflected wavelength ($\Delta\lambda = 290$ nm at 100% strain) than that observed during uniaxial stretching (Figure 4c-i). In particular, the sample underwent failure at 125% elongation owing to the considerably faster decrease in sample thickness than that observed in uniaxial stretching (Figure S13, Supporting Information). In the sample biaxially stretched at 50% strain, the reflected wavelength of the CLCE observed at oblique angles followed a similar optical trend to that of the uniaxial stretching conducted perpendicular to the printing axis, indicating a minimal change in the slant angle during stretching (Figure 4c-ii).

2.5. Morphological Evolution During Stretching

To further investigate the microstructural changes of the printed CLCEs during stretching, wide-angle X-ray scattering (WAXS) analysis was performed in the normal-to-plane geometry under different stretching conditions at various strains (**Figure 5**). An isotropic ring pattern was obtained at $q_i = 1.10$ Å^{-1} for the unstretched CLCE, whereas two clearly separated arcs that intensified with increasing strain were observed for the perpendicularly and parallelly stretched samples (Figure 5a,b). Additionally, 1D azimuthal scan profiles acquired at $q_i = 1.10$ Å^{-1} confirmed that the mesogens of the CLCE reoriented into a stratified structure owing to the untwisting of their helical structures.[10,25,43–46] The order parameter (S) was calculated for both the parallelly and perpendicularly stretched samples at different strain levels (0%, 50%, and 100%); the obtained values—$S_{0\%} = 0$, $S_{50\%} = 0.18$, and $S_{100\%} = 0.29$—were found to be consistent for each strain. This suggested that the microstructure of the CLCE underwent helical untwisting during both parallel and perpendicular stretching. To further verify the helical untwisting of the CLCE upon uniaxial stretching, POM images were acquired while rotating the sample at 45° intervals under perpendicular or parallel stretching at different strain levels (Figure S14, Supporting Information). The unstrained CLCEs exhibited nearly uniform birefringence regardless of the observation angle (i.e., a circularly uniform configuration when viewed from the top). However, the birefringence of the strained CLCEs gradually disappeared—especially at 0°, 90°, 180°, and 270°—with increasing strain regardless of the stretching direction. These results suggested that all the mesogens in the CLCE tended to align in the direction of the applied uniaxial strain and lost the helical structure.[47] In contrast, the WAXS patterns of the biaxially stretched specimen exhibited a consistent ring shape, albeit with decreasing intensity, and the order parameter remained zero at elongations up to 100% (Figure 5c). This implied that the CLCE retained its helical structure throughout the biaxial stretching.[48]

The stretching-induced microstructural changes of the printed CLCE, based on the findings from UV–vis spectroscopy, WAXS analysis, and POM, have been summarized in **Figure 6**. When the CLCE was uniaxially stretched, its helical structure untwisted and gradually transformed into a stratified structure, whereas the biaxially stretched CLCE maintained its helical structure throughout the elongation. Additionally, the initial slant angle of the CLCE obtained through DIW-based printing decreased substantially when the sample was stretched uniaxially parallel to the printing axis. However, the slant angle did not change appreciably when the CLCE was stretched perpendicularly to the printing direction or biaxially elongated.

2.6. Programmable Mechanochromic Response

The anisotropic mechanochromic properties of the printed CLCE were harnessed to create an optically programmable mechanochromic film. First, a concentric-square-patterned red-reflecting film was printed using CLCE doped with 5.0 wt% S1011. When this film was stretched to 150%, a striking contrast was observed between blue and red reflections (**Figure 7**a and Movie S2, Supporting Information). Specifically, the blue reflection was enhanced at both the top and bottom portions of the film, which corresponded to stretching along the direction perpendicular to the printing trajectory. In contrast, the left and right sections of the film predominantly reflected red light during stretching along the printing axis. This remarkable color contrast was due to the significant differences in the extent of blue

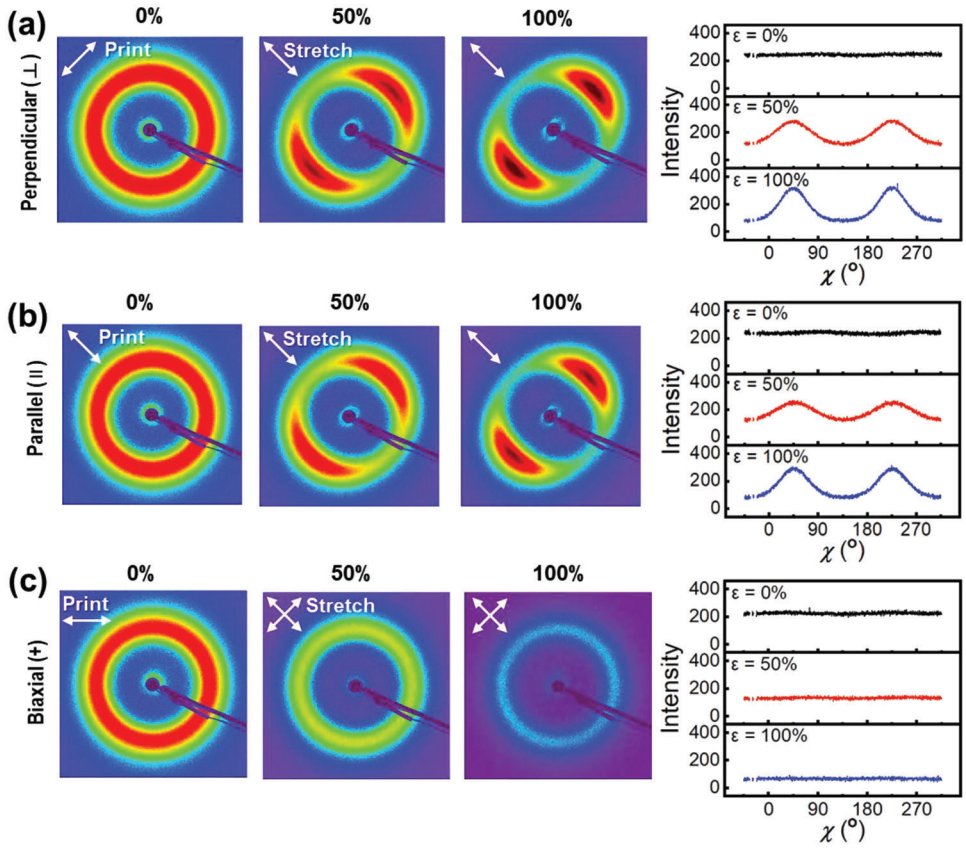

Figure 5. 2D WAXS patterns of uniaxially printed CLCE doped with 5.0 wt% S1011 subjected to different stretching conditions, and the corresponding azimuthal scan profiles at $q_i = 1.10$ Å^{-1}: a) uniaxial stretching (0, 50, and 100%) conducted (a) perpendicular and b) parallel to the printing direction, and c) biaxial stretching (0, 50, and 100%).

shift that occurred when the printed CLCE film was stretched parallel or perpendicular to the printing direction, as discussed previously. Interestingly, when observed between crossed polarizers at a 0-degree rotation, the stretched regions parallel to the printing direction appear dark due to untwisting of cholesteric helix and transformation into a quasi-monodomain structure (Figure S15, Supporting Information). On the other hand, the stretched regions perpendicular to the printing direction still exhibit reflective colors. Such difference in optical properties is perhaps because of easier and complete reorientation of nematic director when stretching in parallel to the printing direction, whereas the reorientation is constrained and incomplete when stretching perpendicular to the printing direction, due to resistance imposed by adjacent domains.

The remarkable color contrast was subsequently exploited to create an encryptable photonic film. To that end, a CLCE film with the initials of Pusan National University—"P," "N," and "U"—was printed, with the printing direction orthogonal to that of the background (Figure 7b). When the film was stretched perpendicular to the printing direction of the letters by 150%, the blue reflection of the letters "P," "N," and "U" became prominent, while the red reflection was displayed by the background (Figure 7b and Movie S3, Supporting Information). The distinct color contrast between the unstretched and stretched states as well as the viewing-direction dependence of the fabricated photonic film can potentially be leveraged to develop encrypted or anticounterfeiting devices.

3. Conclusion

A direct-ink-written CLCE that exhibited intriguing optical and mechanochromic properties in an anisotropic manner was developed in this study. The DIW process enabled tilting of the helical axis of the CLCE, leading to either a blue or red shift of the reflection band depending on the viewing direction relative to the printing trajectory. Notably, an anisotropic mechanochromic response of the printed CLCE was observed for the first time when it was stretched with respect to the printing direction. In particular, the blue shift in the reflected wavelength was more pronounced when the sample was stretched perpendicular to the printing direction than that when it was stretched along the printing trajectory. The smaller blue shift in the latter was attributed to the reorientation of the helices from slanted to upright configurations during the stretching. Leveraging its anisotropic mechanochromic response, the printed CLCE was used to develop a unique strain sensor capable of displaying programmable reflection colors. Overall, the anisotropic structural coloration and mechanochromism of the printed CLCE, in combination with the design flexibility provided by DIW, can show remarkable promise for enabling the utilization of CLCEs in settings such as

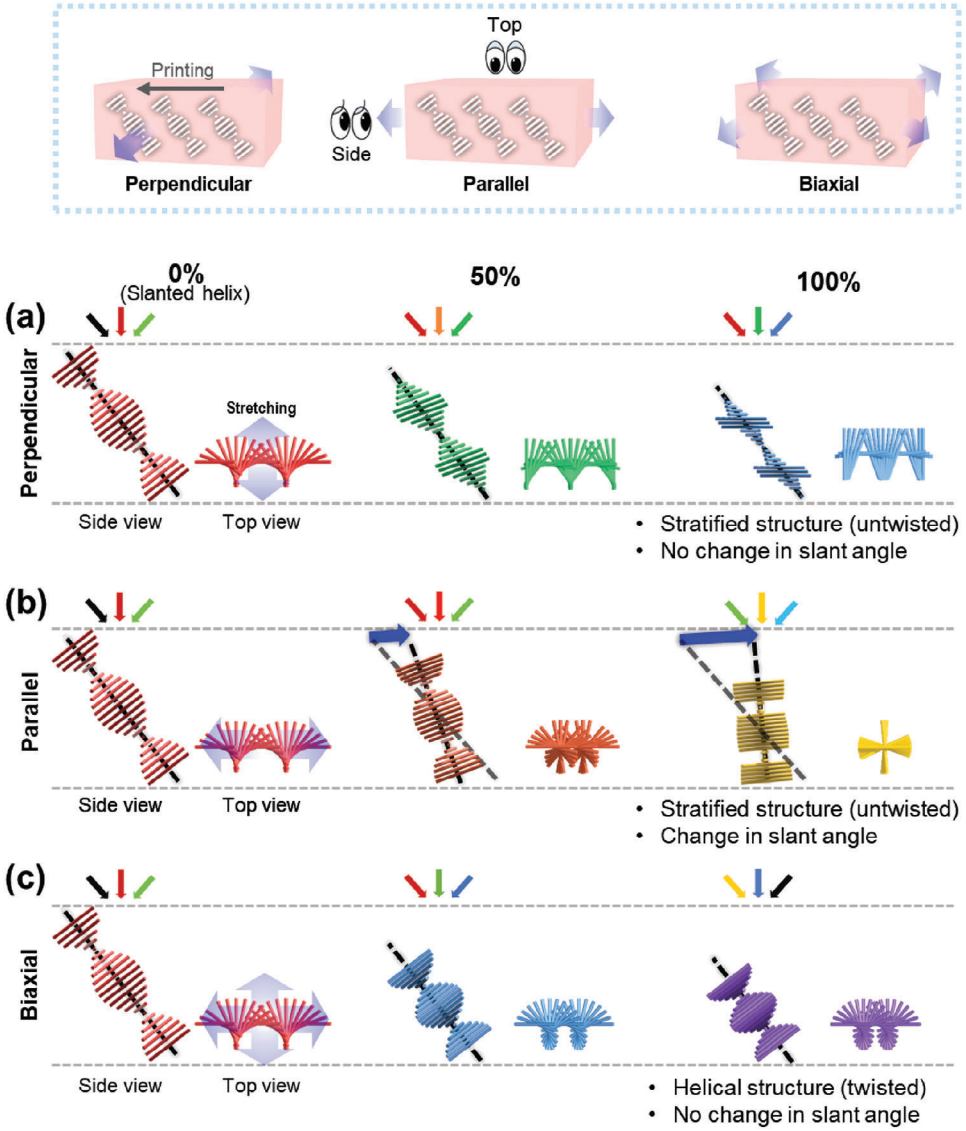

Figure 6. Microstructural evolution of printed CLCE film subjected to different stretching modes: uniaxial stretching performed a) perpendicular and b) parallel to the printing direction, and c) biaxial stretching. Mesogens in the uniaxially stretched films reorient into a stratified structure, whereas those in the biaxially stretched film remain in the helicoidal orientation.

encryption, anticounterfeiting, structural health monitoring, and architectural decoration.

4. Experimental Section

Materials: 2-Methyl-1,4-phenylenebis[4-(3-(acryloyloxy)propoxy)benzoate] (RM257) was purchased from Wilshire Technologies. Benzoic acid, 4-(trans-4-pentylcyclohexyl)-(1S)−1-phenyl-1,2-ethanediyl ester (S1011) was purchased from Jiangsu Hecheng Chemicals and Materials. *n*-Hexylamine was purchased from ACROS. 2,2-Dimethoxy-1,2-diphenylethan-1-one (I-651) was donated by BASF Corporation. All reagents were used without further purification.

Preparation of Printed CLCE Film: CLC ink was synthesized by chain extending the LC monomer (RM257) with *n*-hexylamine through aza-Michael-addition-based step-growth polymerization. The RM257/*n*-hexylamine molar ratio was set at 1.02:1, and the weight percentage of I-651 was fixed at 1.5 wt% of the total CLC mixture. The content of the chiral dopant (S1011) in the CLC mixture was adjusted according to the target reflected wavelength (i.e., 5.0 and 6.2 wt% for reflecting red and green, respectively). A CLC mixture containing RM257 (1000 mg, 1.70 mmol), *n*-hexylamine (168.5 mg, 1.67 mmol), S1011 (62.5 mg), and I-651 (18.8 mg) was added to a 10 mL syringe and thoroughly mixed by vortexing while applying external heat with a heat gun. Thereafter, the CLC mixture was oligomerized by placing it inside a convection oven at 50 °C (that was, in the chiral nematic state) for 20 h. After oligomerization, the viscous CLC ink was further heated to 115 °C for 3 min to ensure complete dissolution of the crystallized chiral dopant into the LC matrix.

DIW of CLC ink was conducted using a 3D printer (Dr. INVIVO 4D, Rokit Healthcare) equipped with a hot-melt extruder containing a 0.2-mm-diameter nozzle. CLC ink was printed on a poly(vinyl alcohol) (PVA)-coated glass slide according to a programmed G-code (NewCreatorK). The PVA coating was used to conveniently remove the sample from the substrate after printing. For PVA coating, a glass slide was cleaned with acetone,

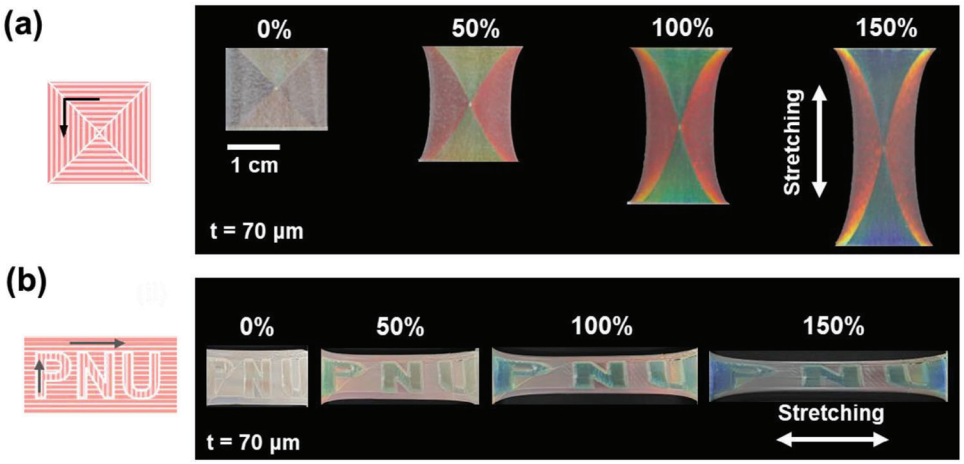

Figure 7. a) Printing path of a CLCE film with a concentric square configuration (left), and photographs of the printed film subjected to various strain levels ranging from 0% to 150% (right). b) Printing path of the CLCE film embedded with the letters "P," "N," and "U" (left), with the printing directions of the letters and background being orthogonal to each other, and photographs of the resulting CLCE film subjected to different strain levels from 0% to 150% (right).

treated with O_2 plasma for 10 min, spin-coated with 4 wt% PVA solution (aq.), and then thermally annealed at 100 °C for 5 min. Printing was performed at 75 °C at a rate of 9 mm s^{-1}. The thickness of the printed sample was controlled by varying the pressure from 100 to 700 kPa, which affected the amount of extrusion. After printing, the sample was annealed on a hot plate at 40 °C for 10 min to promote uniform arrangement of the helical structure. Finally, the printed ink was UV cured (OmniCure S1500, 365 nm, 3.8 mW cm^{-2}) on the hot plate at 40 °C for 20 min, yielding a CLCE film. This was noted that the CLCE printed with a unidirectional printing path exhibited uniform light reflection, whereas CLCE printed with alternating printing path tended to produce relatively non-uniform light reflection, particularly in larger areas.

Preparation of Planar CLCE Film: Glass slides were cleaned with acetone, sonicated in isopropanol, and then treated with O_2 plasma (Harrick plasma, US/PDC-32G) for 10 min. Subsequently, the obtained glass substrates were spin-coated with a commercially available polyamic acid solution and then positioned on a hot plate at 70 °C for 5 min to eliminate any residual solvent. Thermal imidization was subsequently performed by heating the substrates at 200 °C for 1 h. The polyimide-coated surfaces were polished with a velvet cloth, and the glass layers were assembled in an antiparallel manner with a 36-μm-sized spacer to achieve planar alignment.

The cell was filled with the CLC mixture (RM257, *n*-hexylamine, S1011, and I-651) under capillary action in the isotropic state (80 °C) and oligomerized for 18 h inside a convection oven in the nematic phase (52 °C). After oligomerization, the cell was exposed to UV light (OmniCure S1500, λ = 365 nm, 3.8 mW cm^{-2}) for 30 min for crosslinking, thereby yielding a planar-aligned CLCE film.

Material Characterization: ^{1}H NMR spectra were collected using a Varian 500 MHz spectrometer with $CDCl_3$ as the solvent. Attenuated-total-reflection Fourier-transform infrared (ATR FTIR) spectra were obtained in the wavenumber range of 4000—650 cm^{-1} using a Jasco FTIR-4600 spectrometer. A background spectrum was obtained by recording 64 scans at a resolution of 4 cm^{-1}. DSC (TA Instruments, Discovery DSC 25) was performed using a heating–cooling–heating protocol in which each sample was heated to 150 °C, cooled to −50 °C, and then reheated to 150 °C at a rate of 10°C min^{-1} under nitrogen flow. A polarizing microscope (Nikon Eclipse LV100N POL) equipped with a heating stage (Linkam LTS420) was used to characterize the textures and alignment of the samples. The viscoelastic properties of the samples [7.0 mm (l) × 5.0 mm (w) × 0.1 mm (t)] were determined by DMA (TA instruments, DMA Q850) using a tensile clamp under a temperature ramp. The samples were heated from −50 to 150 °C at a heating rate of 3°C min^{-1} at a constant frequency of 1 Hz, amplitude of 14.0 μm, and preload of 0.01 N. The steady-state shear viscosity of CLC ink was measured using a stress-controlled rheometer (HR20, TA Instruments) equipped with a 25 mm parallel-plate geometry. In these experiments, the samples were placed on the bottom of a Peltier plate, and the viscosity was measured by subjecting the samples to rotational shear between the parallel plates at various temperatures. The shear rate was gradually increased from 0.1 to 100 s^{-1} during the measurements. Stress–strain measurement was performed using a universal testing machine (Dr TECH, DR-100) at room temperature with samples measuring 20 mm (l) × 20 mm (w) × 0.1 mm (t) at an elongation rate of 25 mm min^{-1}. A Canon EOS Rebel T3 camera (Canon EF 100 nm macro lens, 1:2/8 USM) was used to capture images and videos of the CLCEs. UV–vis spectra were recorded using a fiber optic spectrometer (Ocean Insight FLAME-T-XR1-ES) in transmission mode with a deuterium–tungsten halogen light source (Ocean Insight DH-2000-BAL) at room temperature. Note that a thin layer of silicone oil was applied onto the surface to minimize light scattering during the UV–vis measurements.

Gel Fraction Analysis: The samples were immersed in chloroform for 48 h to extract uncrosslinked parts and subsequently dried for 24 h in a vacuum oven at ambient temperature. The mass of the sample was measured before and after extraction, and the gel fraction (G) was calculated as follows:

$$G\ (\%) = \frac{m_f}{m_i} \times 100\ (\%) \tag{4}$$

where m_f and m_i represent the final mass after extraction and drying and the initial mass before extraction, respectively.

WAXS Analysis: WAXS measurements were performed using the 9A U-SAXS beamline at the Pohang Accelerator Laboratory (PAL, Korea) with an X-ray wavelength (λ) and sample-to-detector distance of 1.119 Å (E = 11.08 keV) and 0.22 m, respectively. Scattering patterns of 2D were collected using a 2D charge-coupled-device area detector (Rayonix MX170-HS). The orientation factor (P_2), also known as the order parameter (S), was calculated from azimuthal plots using the following equations:[49]

$$P_2 = S = \frac{3\left\langle cos^2\varphi \right\rangle - 1}{2} = 1 - N^{-1}\frac{3}{2}\int_0^{\frac{\pi}{2}} I(\varphi)$$
$$\left\{ sin^2\varphi + (\sin\varphi)\left(cos^2\varphi\right)\right\} \ln\left[\frac{1+\sin\varphi}{\cos\varphi}\right] d\varphi \tag{5}$$

$$N = \int_0^{\pi/2} I(\varphi)\, d\varphi \quad (6)$$

where $I(\varphi)$ was the azimuthal-angle (φ)-dependent intensity at a constant scattering vector [$q = (4\pi/\lambda)\sin(\theta/2)$].

Supporting Information

Supporting Information is available from the Wiley Online Library or from the author.

Acknowledgements

This study was supported by National Research Foundation of Korea (NRF) grants funded by the Ministry of Science and ICT of the Korean government (RS-2023-00208130, RS-2023-00221396, and 2021M3H4A1A03041403). The authors appreciate S.-W.O., H.A. and W.L. for valuable discussions and suggestions.

Conflict of Interest

The authors declare no conflict of interest.

Data Availability Statement

The data that support the findings of this study are available from the corresponding author upon reasonable request.

Keywords

cholesteric liquid crystal elastomers, direct ink writing, mechanochromic materials, photonic crystals, strain sensors

Received: September 5, 2023
Revised: October 20, 2023
Published online:

[1] W. C. Han, Y.-J. Lee, S.-U. Kim, H. J. Lee, Y.-S. Kim, D. S. Kim, *Small* **2023**, *19*, 2206299.
[2] P. Zhang, X. Shi, A. P. H. J. Schenning, G. Zhou, L. T. De Haan, *Adv. Mater. Interfaces* **2020**, *7*, 1901878.
[3] G. Bae, M. Seo, S. Lee, D. Bae, M. Lee, *Adv. Mater. Technol.* **2021**, *6*, 2100479.
[4] A. Tabatabaeian, S. Liu, P. Harrison, E. Schlangen, M. Fotouhi, *Compos. Part A Appl. Sci. Manuf.* **2022**, *163*, 107236.
[5] M. Moirangthem, A. P. H. J. Schenning, *ACS Appl. Mater. Interfaces* **2018**, *10*, 4168.
[6] Y. Guo, H. Shahsavan, M. Sitti, *Adv. Opt. Mater.* **2020**, *8*, 1902098.
[7] Q. Zhu, K. Van Vliet, N. Holten-Andersen, A. Miserez, *Adv. Funct. Mater.* **2019**, *29*, 1808191.
[8] D. Y. Kim, S. Choi, H. Cho, J.-Y. Sun, *Adv. Mater.* **2019**, *31*, 1804080.
[9] Y. Xia, B. Chen, S. Gao, Y. Liu, Z. Zeng, M. Cao, S. Wang, *Adv. Mater. Interfaces* **2019**, *6*, 1901363.
[10] O. Kose, A. Tran, L. Lewis, W. Y. Hamad, M. J. Maclachlan, *Nat. Commun.* **2019**, *10*, 510.
[11] M. E. Mcconney, M. Rumi, N. P. Godman, U. N. Tohgha, T. J. Bunning, *Adv. Opt. Mater.* **2019**, *7*, 1900429.
[12] G. Chen, W. Hong, *Adv. Opt. Mater.* **2020**, *8*, 2000984.
[13] M. T. Brannum, A. M. Steele, M. C. Venetos, L. T. J. Korley, G. E. Wnek, T. J. White, *Adv. Opt. Mater.* **2019**, *7*, 1801683.
[14] S. Nam, D. Wang, G. Lee, S. S. Choi, *Nanophotonics* **2022**, *11*, 2139.
[15] J. A. H. P. Sol, L. G. Smits, A. P. H. J. Schenning, M. G. Debije, *Adv. Funct. Mater.* **2022**, *32*, 2201766.
[16] R. Chen, D. Feng, G. Chen, X. Chen, W. Hong, *Adv. Funct. Mater.* **2021**, *31*, 2009916.
[17] C.-K. Chang, C. M. W. Bastiaansen, D. J. Broer, H.-L. Kuo, *Adv. Funct. Mater.* **2012**, *22*, 2855.
[18] H. Finkelmann, S. T. Kim, A. Muñoz, P. Palffy-Muhoray, B. Taheri, *Adv. Mater.* **2001**, *13*, 1069.
[19] A. M. Martinez, M. K. Mcbride, T. J. White, C. N. Bowman, *Adv. Funct. Mater.* **2020**, *30*, 2003150.
[20] P. V. Shibaev, P. Rivera, D. Teter, S. Marsico, M. Sanzari, V. Ramakrishnan, E. Hanelt, *Opt. Express* **2008**, *16*, 2965.
[21] S.-U. Kim, Y.-J. Lee, J. Liu, D. S. Kim, H. Wang, S. Yang, *Nat. Mater.* **2022**, *21*, 41.
[22] P. Zhang, M. G. Debije, L. T. De Haan, A. P. H. J. Schenning, *ACS Appl. Mater. Interfaces* **2022**, *14*, 20093.
[23] S. ?. T. Kim, H. Finkelmann, *Macromol. Rapid Commun.* **2001**, *22*, 429.
[24] R. Kizhakidathazhath, Y. Geng, V. S. R. Jampani, C. Charni, A. Sharma, J. P. F. Lagerwall, *Adv. Funct. Mater.* **2020**, *30*, 1909537.
[25] J. Ma, Y. Yang, C. Valenzuela, X. Zhang, L. Wang, W. Feng, *Angew. Chem., Int. Ed.* **2021**, *61*, e202116219.
[26] J. A. H. P. Sol, H. Sentjens, L. Yang, N. Grossiord, A. P. H. J. Schenning, M. G. Debije, *Adv. Mater.* **2021**, *33*, 2103309.
[27] J. A. H. P. Sol, R. F. Douma, A. P. H. J. Schenning, M. G. Debije, *Adv. Mater. Technol.* **2023**, *8*, 2200970.
[28] T. H. Ware, M. E. Mcconney, J. J. Wie, V. P. Tondiglia, T. J. White, *Science* **2015**, *347*, 982.
[29] J. Lee, Y. Guo, Y.-J. Choi, S. Jung, D. Seol, S. Choi, J.-H. Kim, Y. Kim, K.-U. Jeong, S.-K. Ahn, *Soft Matter* **2020**, *16*, 2695.
[30] Y. Lee, S. Choi, B.-G. Kang, S.-K. Ahn, *Materials* **2020**, *13*, 3094.
[31] C. P. Ambulo, J. J. Burroughs, J. M. Boothby, H. Kim, M. R. Shankar, T. H. Ware, *ACS Appl. Mater. Interfaces* **2017**, *9*, 37332.
[32] A. Kotikian, R. L. Truby, J. W. Boley, T. J. White, J. A. Lewis, *Adv. Mater.* **2018**, *30*, 1706164.
[33] K. Kim, Y. Guo, J. Bae, S. Choi, H. Y. Song, S. Park, K. Hyun, S.-K. Ahn, *Small* **2021**, *17*, e2100910.
[34] K. F. Wissbrun, *J. Rheol.* **1981**, *25*, 619.
[35] P. T. Mather, A. Romo-Uribe, C. D. Han, S. S. Kim, *Macromolecules* **1997**, *30*, 7977.
[36] G. E. Bauman, J. A. Koch, T. J. White, *Soft Matter* **2022**, *18*, 3168.
[37] Z.-G. Zheng, Y. Li, H. K. Bisoyi, L. Wang, T. J. Bunning, Q. Li, *Nature* **2016**, *531*, 352.
[38] A. Komp, J. Rühe, H. Finkelmann, *Macromol. Rapid Commun.* **2005**, *26*, 813.
[39] H. K. Bisoyi, T. J. Bunning, Q. Li, *Adv. Mater.* **2018**, *30*, 1706512.
[40] H. Nagai, X. Liang, Y. Nishikawa, K. Nakajima, K. Urayama, *Macromolecules* **2016**, *49*, 9561.
[41] A. J. J. Kragt, N. C. M. Zuurbier, D. J. Broer, A. P. H. J. Schenning, *ACS Appl. Mater. Interfaces* **2019**, *11*, 28172.
[42] P. Zhang, A. J. J. Kragt, A. P. H. J. Schenning, L. T. De Haan, G. Zhou, *J. Mater. Chem. C* **2018**, *6*, 7184.
[43] M. Warner, E. M. Terentjev, R. B. Meyer, Y. Mao, *Phys. Rev. Lett.* **2000**, *85*, 2320.
[44] Y. Mao, E. M. Terentjev, M. Warner, *Phys. Rev. E* **2001**, *64*, 041803.
[45] P. Cicuta, A. R. Tajbakhsh, E. M. Terentjev, *Phys. Rev. E* **2002**, *65*, 051704.
[46] C. L. C. Chan, M. M. Bay, G. Jacucci, R. Vadrucci, C. A. Williams, G. T. Van De Kerkhof, R. M. Parker, K. Vynck, B. Frka-Petesic, S. Vignolini, *Adv. Mater.* **2019**, *31*, 1905151.
[47] J. Schmidtke, S. Kniesel, H. Finkelmann, *Macromolecules* **2005**, *38*, 1357.
[48] C. Kwon, S. Nam, S. H. Han, S. S. Choi, *Adv. Funct. Mater.* **2023**, 2304506.
[49] M. Deutsch, *Phys. Rev. A* **1991**, *44*, 8264.